Ultrasonics Sonochemistry 107 (2024) 106892

Contents lists available at ScienceDirect

Ultrasonics Sonochemistry

journal homepage: www.elsevier.com/locate/ultson

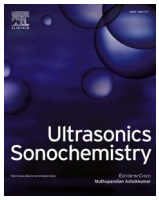

Preparation of protein-stabilized Litsea cubeba essential oil nano-emulsion by ultrasonication: Bioactivity, stability, *in vitro* digestion, and safety evaluation

Qiang Peng [a], Zhiwu Huang [a], Guixin Liang [a], Yongguang Bi [a,b,c,d,*], Fansheng Kong [a], Zhong Wang [d], Shaofan Tan [c], Junyong Zhang [e]

[a] *School of Pharmacy, Guangdong Pharmaceutical University, China*
[b] *Guangdong Provincial Key Laboratory of Advanced Drug Delivery, Guangdong Provincial Engineering Center of Topical Precise Drug Delivery System, Guangdong Pharmaceutical University, China*
[c] *Guangdong Dongshenglin Pharmaceutical Co., Ltd, China*
[d] *Yunfu Traditional Chinese Medicine Hospital, China*
[e] *Guangzhou Aobo Industrial Innovation Service Co., Ltd, Guangzhou 510670, China*

ARTICLE INFO

Keywords:
Litsea cubeba essential oil
Nano-emulsion
Ultrasonication
Bioactivity
In vitro digestion
Safety evaluation

ABSTRACT

Litsea cubeba essential oil (LCEO) has garnered widespread attention due to its robust biological activity. However, challenges such as high volatility, limited water solubility, and low bioavailability impede its application. Nano-emulsion encapsulation technology offers an effective solution to these issues. In this study, we prepared litsea cubeba essential oil nano-emulsion (LCEO-NE) for the first time using whey protein (WP) as the emulsifier through an ultrasonic-assisted method, achieving high efficiency with minimal energy consumption. Transmission electron microscopy and dynamic light scattering analyses revealed that the nanoparticles were uniformly spherical, with a particle size of 183.5 ± 1.19 nm and a zeta potential of −35.5 ± 0.95 mV. Stability studies revealed that LCEO-NE exhibited excellent thermal and salt stability, maintaining its integrity for up to four weeks when stored at 4 °C and 25 °C. *In vitro* digestion assays confirmed the digestibility of LCEO-NE. Furthermore, evaluation of the DPPH, ABTS, and antimicrobial activities revealed that LCEO-NE displayed superior bacteriostatic and antioxidant properties compared to LCEO. Scanning electron microscopy elucidated that its bacteriostatic effect involved the disruption of bacterial microstructure. Hemocompatibility and cytotoxicity assays demonstrated the safety of LCEO-NE within the effective concentration range. This research supports the utilization of nanoparticles for encapsulating LCEO, thereby enhancing its stability and bioactivity, and consequently expanding its applications in the food and pharmaceutical industries.

1. Introduction

Litsea cubeba (LC), commonly known as mountain pepper, wild pepper, or wood ginger, belongs to the Lauraceae family, mainly distributed in tropical and subtropical regions [1]. Litsea cubeba essential oil (LCEO) is traditionally utilized in China as a culinary spice oil, lending a fresh lemony and spicy aroma to dishes [2]. Additionally, LCEO contains a wide range of pharmacologically active components, including citral, limonene, linalool, lauric acid, citronellal, and pinene [3]. These compounds contribute to its diverse pharmacological activities, such as antioxidant, antimicrobial, anti-inflammatory, antidiabetic, anticarcinogenic, insecticidal, and antiallergic effects [4].

However, the practical application of LCEO is often limited by challenges like poor solubility, rapid volatilization, environmental degradation, and photosensitivity [5]. Nano-emulsification technique, with water acting as the continuous phase facilitating the dispersion of oil into minuscule droplets, has been effective in addressing these challenges [6]. Several researchers have reported applications of this technology in essential oils. For instance, Christaki et al. prepared oregano oil nano-emulsion with uniform taste and texture, mitigating potential irritation from the volatile oil [7]. Garzoli et al. found that lavender essential oil, after nano-emulsified, exhibited stabilized and slow release, extending its applications in food and pharmaceuticals [8]. Furthermore, Liang et al. observed that formulating cinnamon essential

* Corresponding author at: School of Pharmacy, Guangdong Pharmaceutical University, Guangzhou 510006, Guangdong, China.
E-mail address: biyongguang2002@163.com (Y. Bi).

https://doi.org/10.1016/j.ultsonch.2024.106892
Received 2 March 2024; Received in revised form 16 April 2024; Accepted 28 April 2024
Available online 29 April 2024

oil into nano-emulsion heightened its interaction with biological systems, resulting in enhanced antioxidant and antimicrobial activities [9]. Recent trends have favored food-grade proteins in nano-emulsion preparation. Among these, whey protein (WP) is prominent due to its excellent emulsification properties, amphiphilicity, and water solubility, surpassing traditional inorganic emulsifiers in biocompatibility and biosafety [10]. Zhang et al. reported that sea buckthorn fruit oil nano-emulsion prepared using WP as an emulsifier was exceptionally safe and stable [11]. Therefore, it can be hypothesized that encapsulating LCEO in nano-emulsion could enhance its stability, bioactivity, and safety. Nonetheless, only a few studies have evaluated the activity and safety of LCEO after nano-emulsification.

Ultrasound-assisted preparation is a widely used high-energy method for nano-emulsion production [12]. This technique utilizes the mechanical vibration and cavitation effects of ultrasound to generate and collapse bubbles in the liquid medium, effectively shearing the phase-soluble liquid into fine droplets [13]. Emulsifiers like WP rapidly adsorb at the droplet interface to prevent recoalescence [14]. In comparison to high-pressure homogenization (HPH), ultrasound-assisted preparation offers greater adaptability, simplicity, and significant energy efficiency [15].

In this research, we utilized the ultrasound-assisted method with WP as an emulsifier to prepare LCEO nano-emulsion. Our investigation aimed to determine the optimum conditions for preparing LCEO-NE, analyze its morphology using characterization techniques, and assess digestion through *in vitro* experiments. Additionally, we conducted evaluations on the temperature, pH, salinity, storage stability, and safety of the emulsion. Furthermore, we determined its antioxidant and antimicrobial capacities while thoroughly investigating the antimicrobial mechanism.

2. Materials and methods

2.1. Materials and chemicals

LCEO was obtained from Yuanye Biotechnology Co., Ltd. (Shanghai, China). Whey Protein (WP), with a certified purity of 80%, was purchased from Macklin Biochemical Co., Ltd. (Shanghai, China). LO2 liver cells were sourced from the Shanghai Cell Bank of the Chinese Academy of Sciences (China). DPPH and ABTS were purchased from Aladdin Biochemical Technology Co., Ltd. (Shanghai, China). Fuzhou Phygene Biotechnology Co., Ltd. (Fujian, China) provided Simulated Salivary Fluid (SSF), Simulated Gastric Fluid (SGF), and Simulated Intestinal Fluid (SIF). (*Staphylococcus aureus* (*S. aureus*) CMCC 26003, *Escherichia coli* (*E. coli*) CMCC 44102, *Pseudomonas aeruginosa* (*P. aeruginosa*) CMCC 10104, *Bacillus subtilis* (*B. subtilis*) CMCC (B) 63501, *Salmonella typhimurium* (*S. typhimurium*) CMCC 50094) were obtained from the Guangdong Institute of Microbiology (Guangzhou, China). All other chemical reagents used in this study were of analytical grade and deionized water was used throughout the experiments.

2.2. Chemical analysis of LCEO

Slightly modified from a previous study [16], GC–MS (Agilent 7890B gas chromatography and Agilent 5977 mass spectrometer, CA, USA) was utilized to analyze the chemical component of LCEO. The initial column temperature was set at 50 °C for 2 min, then increased to 120 °C at a rate of 3 °C/min. After 2 min, the temperature was further increased to 250 °C at a rate of 15 °C/min and held for 5 min. The column flow rate was 1 mL/min. The injection, quadrupole, and ionization temperatures were set at 220 °C, 150 °C, and 230 °C, respectively. The photomultiplier voltage was set to 1024 V. The mass scan range was selected from 30 to 550 AMU. Peaks were identified and analyzed using the Nist147 technique library.

2.3. Preparation of LCEO-NE under different conditions

Slightly modified from the literature [17], the WP solution was stirred for 2 h, followed by refrigeration at 4 °C for 12 h to enhance emulsification effectiveness, after which LCEO was incorporated into the protein solution at a ratio of 1:10 (w/v) and emulsified using a high-speed Ultra-Turrax mixer (T25, IKA, Germany) at 16,000 rpm for 5 min, resulting in a micro-emulsion. This micro-emulsion was then converted into a nano-emulsion through ultrasonic homogenization (SCIENTZ-IID, 6 mm, Ningbo, China) in an ice bath. The optimization of nano-emulsion properties involved adjusting the WP concentration (2–5%), ultrasonic time (5–20 min), and ultrasonic power (90–450 W).

2.4. Characterization of nano-emulsion

The zeta potential (ZP), particle size, and polymer dispersion index (PDI) of LCEO-NE were determined at 25 °C using a Delsa Nanometer zeta potential/particle size analyzer (Delsa Nano C, USA). To avoid multiple scattering effects, the nano-emulsion was diluted 200 times [18]. The initial morphology of LCEO-NE and its state after simulated gastrointestinal digestion were observed using scanning electron microscopy (SEM) (Zeiss Sigma 300, Germany) [19]. Additionally, the morphology and structure of LCEO-NE were investigated post-staining with 2% phosphotungstic acid using a transmission electron microscope (TEM) (JEM-1400 plus, Japan) [20].

2.5. Determination of rheological property

According to the relevant literature [21], the rheological property of LCEO-NE was assessed using a DHR-3 rheometer (TA Instruments, USA). The viscosity was determined by measuring the shear rate ranging from 0.01 to 200 s^{-1} at 25 °C.

2.6. Physicochemical stability measurements

2.6.1. Determination of physical stability

The centrifugal stabilization constant (Ke) was measured based on the existing literature with some modifications [22]. The absorbance of LCEO-NE (diluted 100 times) before and after centrifugation (2200 rpm) was measured at 500 nm using a UV–visible spectrophotometer (UV-5500PC, Shanghai, China). Ke indicates the centrifugal stability of LCEO-NE was calculated as Eq. (1):

$$\text{Ke}\ (\%) = \frac{A - A_1}{A} \times 100\% \quad (1)$$

where A and A_1 represent the absorbance values of the diluted LCEO-NE before and after centrifugation, respectively.

2.6.2. Thermal stability assessment

LCEO-NE samples were subjected to 45, 60, 75, and 90 °C for 30 min. After returning to room temperature, parameters such as particle size, ZP, and Ke were measured.

2.6.3. PH stability examination

The pH of LCEO-NE was adjusted to 3, 5, 7, and 9 using 0.1 M HCl/NaOH, followed by property assessments.

2.6.4. Salinity stability evaluation

LCEO-NE was mixed in equal volumes with NaCl solutions of varying concentrations (60, 120, 180, and 240 mM). Measurements of the properties were conducted after 12 h of refrigeration.

2.6.5. Storage stability investigation

LCEO-NE was stored at 4 °C and 25 °C for 4 weeks, with weekly assessments for particle size.

2.7. Simulated gastrointestinal digestion

LCEO-NE, pre-warmed to 37 °C, was subjected to a digestive environment that mimics the oral, gastric, and intestinal phases of digestion [23].

2.7.1. Oral phase

Simulated Salivary Fluid (SSF) with 3.5 mg/mL amylase concentration was pre-heated to 37 °C for 5 min, then mixed with LCEO-NE at a 1:1 mass ratio, adjusted to pH 6.8 and shaken at 100 rpm for 5 min at 37 °C to simulate oral condition. Post-reaction, samples were extracted to analyze particle size and morphology.

2.7.2. Gastric phase

Simulated Gastric Fluid (SGF) containing 3.5 mg/mL pepsin was pre-warmed to 37 °C for 5 min, then mixed with the orally digested LCEO-NE solution at a 1:1 mass ratio, adjusted to pH 2.5 and shaken at 100 rpm for 2 h at 37 °C to simulate gastric condition. Samples were collected at intervals (0, 0.5, 1, 1.5, and 2 h) for particle size determination, with morphology examined at the end of digestion.

2.7.3. Intestine phase

Simulated Intestinal Fluid (SIF), containing 3.5 mg/mL trypsin, 3.5 mg/mL pancreatic lipase, and 5 mg/mL bile salts, was pre-warmed to 37 °C for 5 min, then mixed with the gastrically digested sample solution at a 1:1 mass ratio, adjusted to pH 7 and shaken at 100 rpm for 2 h at 37 °C to simulate intestinal conditions. Samples were taken at intervals (0, 0.5, 1, 1.5, and 2 h) for particle size determination, with morphology observed at the end of digestion.

2.8. Measurement of antioxidant capacities

2.8.1. DPPH radicals scavenging activity

Slightly adapted from the literature [24], a 2 mL sample solution (0.5, 1, 1.5, 2, and 2.5 mg/mL) was mixed with an equal volume of DPPH ethanol solution (0.1 mM). The reaction proceeded for 30 min at room temperature, shielded from light. Absorbance at 517 nm was measured post-reaction. Vc and WP served as positive and blank controls, respectively. The DPPH radical scavenging rate was calculated as Eq. (2):

$$DPPH\ radical\ scavenging\ activity\ (\%) = \left(1 - \frac{A_1 - A_2}{A_0}\right) \times 100\% \quad (2)$$

where A_1 is the absorbance of the DPPH ethanol solution and sample mixture; A_2 is the absorbance of the solvent and sample mixture; A_0 is the absorbance of the solvent and DPPH ethanol solution mixture.

2.8.2. ABTS radicals scavenging activity

According to the relevant literature, it has been modified [25]. ABTS stock solution (7 mmol/L, 1 mL) was mixed with $K_2S_2O_8$ solution (140 mmol/L, 88 μL) and left overnight at room temperature, protected from light. The solution was then diluted with PBS (0.2 M, pH 7.4) until the absorbance at 734 nm was 0.70 ± 0.02, forming the ABTS working solution. For the assay, 3 mL of the ABTS working solution was mixed with 1 mL of the sample solution (0.5, 1, 1.5, 2, and 2.5 mg/mL). The reaction proceeded in the dark for 6 min, and absorbance at 734 nm was measured post-reaction. Vc and WP served as positive and blank controls, respectively. The ABTS free radical scavenging rate was determined as Eq. (3):

$$ABTS\ radical\ scavenging\ activity\ (\%) = \left(1 - \frac{A_1 - A_2}{A_0}\right) \times 100\% \quad (3)$$

where A_1 is the absorbance of the ABTS radical and sample mixture; A_2 is the absorbance of the solvent and sample mixture; A_0 is the absorbance of the solvent and ABTS radical mixture.

2.9. Evaluation of antibacterial qualities

2.9.1. Determination of minimum inhibitory concentration (MIC) and minimum bactericidal concentration (MBC)

LCEO-NE and LCEO were diluted using the twofold dilution method in Mueller-Hinton broth (MHB) [26]. Typically, 50 μL of bacterial culture (10^6 CFU/mL) (*S. aureus*, *S. typhimurium*, *B. subtilis*, *P. aeruginosa*, and *E. coli*) was mixed with 100 μL of the diluted sample in a 96-well cell culture plate and incubated at 37 °C for 18–24 h. Following this, 20 μL of 0.2 g/L Iodonitrotetrazolium chloride (INT) solution was introduced to each well as a color developer and incubated for an additional 6 h. The first well to exhibit a color change was recorded as the MIC. Levofloxacin and WP were used as positive and blank controls, respectively. For MBC determination, cultures from non-discolored wells were transferred to MHA medium and incubated at 37 °C for 24 h. The lowest concentration showing no bacterial growth in the plate was identified as the MBC.

2.9.2. Determination of bacterial growth curves

A 96-well plate was utilized to combine 100 μL of media containing the MIC of the sample with 50 μL of bacterial solution (10^5–10^6 CFU/mL). This mixture was incubated at 37 °C for 24 h, with absorbance measurements at 600 nm taken every 2 h [27]. Blank control contained media only, while 2% DMSO and levofloxacin served as negative and positive controls, respectively.

2.9.3. Antibacterial mechanism

2.9.3.1. Determination of the absorbance of bacterial extracellular nucleic acids. A mixture of 4 mL MIC sample and 2 mL bacterial solution (10^5–10^6 CFU/mL) was incubated at 37 °C for 6 h, then centrifuged at 5000 rpm for 6 min [28]. The absorbance of the supernatant was measured at 260 nm, with saline used as the blank control and 2% DMSO as the negative control.

2.9.3.2. Determination of the contents of bacterial extracellular polysaccharides. A glucose standard curve was established using the phenol–sulfuric acid method [29]. The supernatant from 2.9.3.1 was analyzed using this method to determine the polysaccharide content.

2.9.3.3. Determination of the contents of bacterial extracellular soluble proteins. A standard curve for bovine serum albumin (BSA) was generated using the Coomassie Brilliant Blue method [30]. The supernatant from 2.9.3.1 was analyzed using this method to determine the soluble protein content.

2.9.3.4. Bacterial ultrastructure. Samples were incubated with *E. coli* and *S. aureus* (approximately 10^8 CFU/mL) at 37 °C for 6 h. After incubation, the mixtures were centrifuged at 6000 rpm for 5 min. The resultant precipitates were washed thrice with PBS (0.1 M, pH 7.4), fixed overnight with 4% glutaraldehyde at 4 °C, rewashed thrice with PBS, and then fixed for 1 h with 2% glutaraldehyde at 4°C. After additional washing three times, dehydration was performed using graded ethanol series (20%, 50%, 80%, and 100%, each for 10 min) followed by *tert*-butanol substitution [31]. The bacterial structure and morphology were then observed under the SEM.

2.10. Security assessment

2.10.1. Hemocompatibility test

Animals were treated according to the protocol approved by the Ethics Committee of Guangdong Pharmaceutical University, approval number SYXK2022-0125. Rats were euthanized using a euthanasia method after blood sampling and deep anesthesia with tribromoethanol. The blood was washed four times with saline, centrifuged at 1500 rpm for 5 min each time, and then diluted to 2% erythrocyte suspension.

Table 1
Analysis of LCEO main components.

No.	Retention time	Compounds	Molecular formula	Relative percentage
1	4.404	2,3-Butanediol	$C_4H_{10}O_2$	0.108%
2	7.734	α-Phellandrene	$C_{10}H_{16}$	0.092%
3	7.970	α-Pinene	$C_{10}H_{16}$	2.036%
4	8.494	Camphene	$C_{10}H_{16}$	0.419%
5	9.498	β-Phellandrene	$C_{10}H_{16}$	1.670%
6	9.598	β-Pinene	$C_{10}H_{16}$	1.733%
7	10.096	5-Hepten-2-one, 6-methyl-	$C_8H_{14}O$	2.148%
8	10.182	2,3-Dehydro-1,8-cineole	$C_{10}H_{16}O$	0.174%
9	10.245	β-Myrcene	$C_{10}H_{16}$	0.112%
10	10.315	5-Hepten-2-ol, 6-methyl-	$C_8H_{16}O$	0.052%
11	10.979	3-Carene	$C_{10}H_{16}$	0.043%
12	11.520	p-Cymene	$C_{10}H_{14}$	0.025%
13	11.638	o-Cymene	$C_{10}H_{14}$	0.275%
14	11.937	D-Limonene	$C_{10}H_{16}$	19.823%
15	15.007	Linalool	$C_{10}H_{18}O$	0.901%
16	17.430	Citronellal	$C_{10}H_{18}O$	0.551%
17	21.807	β-Citral	$C_{10}H_{16}O$	31.961%
18	22.093	2-Cyclohexen-1-one, 3-methyl-6-(1-methylethyl)-	$C_{10}H_{16}O$	0.301%
19	23.222	α-Citral	$C_{10}H_{16}O$	34.456%
20	25.770	2-Cyclohexen-1-one, 2-methyl-5-(1-methylethyl)-, (S)-	$C_{10}H_{16}O$	0.961%
21	27.545	2,4-Dimethyl-1-hepten-4-ol	$C_9H_{18}O$	1.074%
22	28.580	Nepetalactone	$C_{10}H_{14}O_2$	0.183%
23	29.290	1,2,3-Benzenetriol	$C_6H_6O_3$	0.192%
24	30.969	3,3-Dimethylbutan-2-yl 2-methylbutanoate	$C_{11}H_{22}O_2$	0.141%
25	31.099	4-Methyl-6-(tetrahydropyran-2-yloxy) hex-4-enal	$C_{12}H_{20}O_3$	0.175%
26	36.527	Neric acid	$C_{10}H_{16}O_2$	0.247%

Equal volumes of erythrocyte suspension were mixed with different concentrations of sample solutions (0.5, 1, 1.5, 2, and 2.5 mg/mL), incubated for 1 h at 37 °C in a water bath, and centrifuged for 10 min (1500 rpm). The absorbance of the supernatant was measured at 540 nm. Distilled water and saline were set as positive and negative controls, respectively. The hemolysis rate was calculated using the following Eq. (4):

$$HR\ (\%) = \frac{A_{sample} - A_{negative\ control}}{A_{positive\ control} - A_{negative\ control}} \times 100\% \quad (4)$$

where A_{sample}, $A_{negative\ control}$, and $A_{positive\ control}$ denote the absorbance of the sample, negative control, and positive control, respectively.

2.10.2. Cytotoxicity assay

Cytotoxicity assay was conducted based on a previous study with appropriate modifications [32]. LO2 cells were seeded in 96-well plates at a density of approximately 10^4 cells per well and cultured for 24 h to allow the cells to adhere to the walls of the wells. The medium was then replaced with fresh medium containing varying concentrations of the sample solution and incubated for an additional 12 h. Subsequently, the medium was replaced again with fresh medium containing 10 μL of CCK-8 solution, followed by 1 h incubation. Absorbance at 450 nm was measured, and cell viability was calculated using the following Eq. (5):

$$Cellviability\ (\%) = \frac{A_{sample} - A_{blank}}{A_{control} - A_{blank}} \times 100\% \quad (5)$$

where A_{sample} is the absorbance of each sample group, A_{blank} is the absorbance of the blank group, $A_{control}$ is the absorbance of the control group.

2.11. Statistical analysis

Results were shown as mean ± standard deviation (SD), with each experiment conducted in triplicate. Using Origin 2021 (Origin, USA) for plotting and SPSS 25.0 (IBM, USA) for ANOVA analysis. Differences were considered statistically significant at $p < 0.05$.

3. Results and discussion

3.1. Chemical composition of LCEO

As shown in Table 1, the GC–MS analysis identified 26 chemical constituents in the sample. Predominantly, terpenoids accounted for 94.175% of the constituents. The most abundant component was Citral, comprising α-Citral (34.456%) and β-Citral (31.961%), known for its antimicrobial, anti-inflammatory, and anticarcinogenic properties [33]. D-Limonene, constituting 19.823% of the mixture, exhibited gastrointestinal protective and antimicrobial effects [34]. Additionally, Pinene and Phellandrene were detected, the former noted for its antioxidant and antiviral properties [35], and the latter for its analgesic activity [36]. Notably, the types and contents of the primary chemical components in this study were similar to previous research, although minor constituents showed considerable variation [37,38]. This discrepancy might be attributed to factors such as plant origin, harvesting time, and extraction method.

3.2. Influence of different preparation conditions on LCEO-NE

3.2.1. Influence of emulsifier concentration on LCEO-NE

As depicted in Fig. 1A, the minimum particle size of LCEO-NE was 204.46 ± 2.14 nm and the maximum absolute ZP value was 32.91 ± 1.21 mV. WP, acting as an emulsifier in LCEO-NE, reduces the surface tension of oil droplets due to its surface activity, facilitating the dispersion of droplets and the formation of smaller nano-emulsion structures [10]. A moderate increase in WP concentration enhanced this effect, leading to a more uniform distribution of oil droplets in the aqueous phase, thereby contributing to the formation of smaller

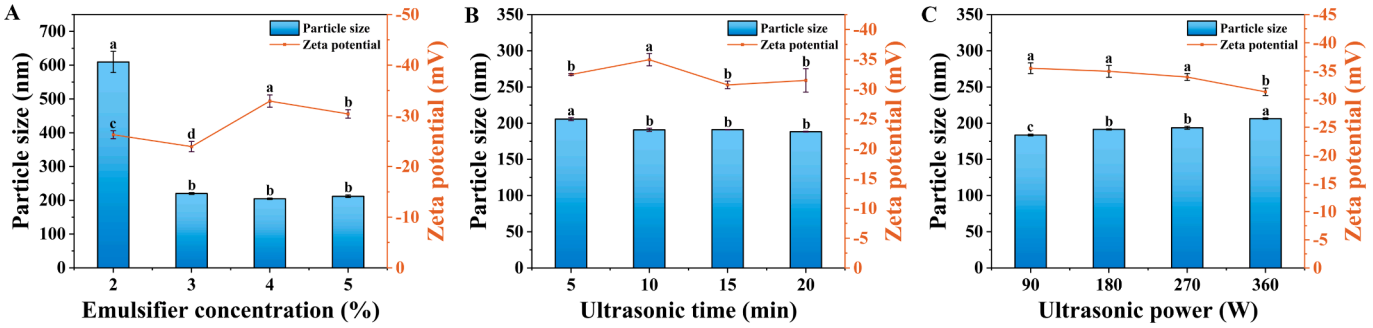

Fig. 1. Preparation of LCEO-NE under different conditions of Emulsifier (A), Ultrasonic time (B), and Ultrasonic power (C). Different lowercase letters indicate significant differences in particle size or zeta potential ($p < 0.05$).

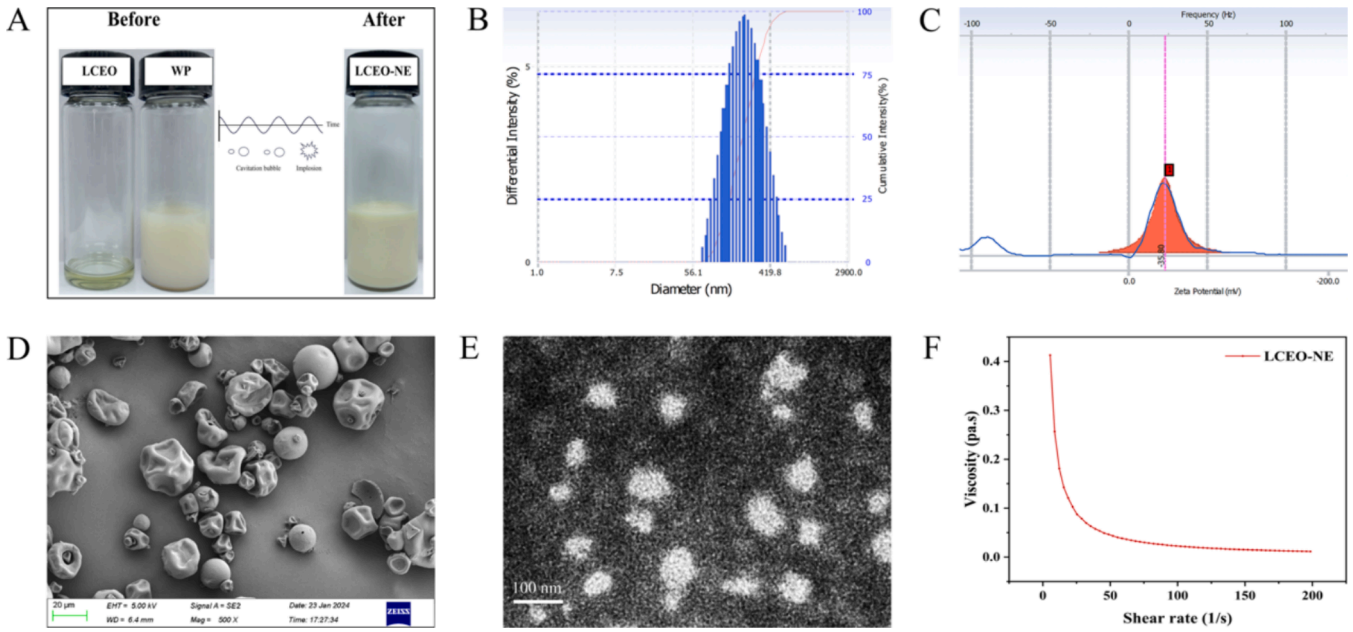

Fig. 2. Particle size distribution (B) and zeta potential distribution (C) of LCEO-NE; SEM image of WP (D) and TEM image of LCEO-NE (E); Rheological characterization of LCEO-NE (F).

nanostructures. However, beyond a certain threshold, WP tended to over-wrap the oil droplets, thickening the protein layer and leading to an increase in nano-emulsion particle size [39]. These results suggest that the concentration of emulsifier significantly affects the stability of the nano-emulsion, with optimal performance observed at a WP concentration of 4%.

3.2.2. *Effect of ultrasonic conditions on LCEO-NE*

As illustrated in Fig. 1B and C, significant variations in particle size and ZP were observed when altering ultrasonic time (from 5 to 20 min) and power (from 90 W to 450 W). The smallest particle size (183.53 ± 1.19 nm) and highest absolute ZP value (35.48 ± 0.95 mV) were achieved with 10 min of sonication at 90 W. Continuing to shorten the sonication time to 5 min, the particle size of the nano-emulsion increased, and the absolute value of ZP decreased. Likely due to the relatively lower transfer of ultrasonic energy to the particles in the liquid, physical effects such as shearing, collision, and vortexing occur with relatively low frequency and intensity, which are not sufficient to activate the WP molecules adequately to allow them to interact with the LCEO and form stable emulsified structures [13]. As a result, some particles remained relatively large and did not reach their minimum size. Further increases in sonication time or power (beyond 10 min and 90 W) also decreased the stability of LCEO-NE. This agrees with the results reported in a previous study [40]. Such a phenomenon can be attributed to the saturation of ultrasound action, where excessive ultrasonic energy may cause the formed nano-emulsion to rupture or recondense. Moreover, prolonged high-power ultrasound induces localized high temperatures and pressures, potentially denaturing WP and reducing their emulsification properties [41]. Therefore, the optimal sonication parameter for the preparation of LCEO-NE is 10 min of sonication at 90 W.

3.3. *Characterization of nano-emulsion*

Nano-emulsion serves as an effective carrier to transform insoluble substances or macromolecular compounds into nanosized entities, significantly enhancing intestinal absorption of active substances [42]. The particle size of LCEO-NE was measured to be less than 200 nm (Fig. 2B), which satisfies the criteria for nano-emulsion. Its particle size distribution followed a normal distribution, indicating consistent and uniform particle sizes [43]. The PDI is a critical metric for assessing the uniformity of particle size distribution in solutions or suspensions. A lower PDI indicates greater uniformity [44]. The PDI of LCEO-NE was determined to be 0.172 ± 0.008, denoting a well-dispersed and relatively uniform distribution. The ZP reflects the surface charge on droplets, with the absolute ZP value correlating to the surface charge intensity. A higher absolute ZP value suggests greater surface charge, leading to increased electrostatic repulsion between particles, which helps maintain dispersion and prevents aggregation [45]. The absolute ZP value of LCEO-NE was greater than 35 mV (Fig. 2C), implying a high degree of stability.

Fig. 2D and E showed the SEM image of WP and TEM image of LCEO-NE, respectively. The internal morphology of WP was irregularly spherical with a particle size of about 10–15 μm, whereas LCEO-NE had a uniform near-spherical distribution with a particle size of about 50–100 nm. However, the droplet size observed via TEM was smaller than the average particle size measured by the laser particle sizer. This difference can be attributed to two factors. Firstly, regarding the contrasting states of LCEO-NE during measurement, the laser particle sizer assesses a diluted nano-emulsion in liquid form, whereas TEM examines a solid-state nano-emulsion formed after drying, the drying process during TEM measurements leads to dehydration, altering droplet size [46]. Secondly, the differences in operating principles between the laser particle sizer (based on scattered light) and transmission electron microscope (based on an electron beam) contribute to variations in observed sizes [47]. Despite these discrepancies, the combined characterizations confirm the successful preparation of the nano-emulsion.

3.4. *Rheological characteristic measurement*

The observed trend demonstrated a significant decrease in the apparent viscosity of the nano-emulsion at shear rates below 50 s^{-1} (Fig. 2F). However, as the shear rates surpass 50 s^{-1}, the reduction in apparent viscosity became less pronounced and gradually approached zero. This behavior can be attributed to the presence of aggregates within the nano-emulsion. Under shear stress, these aggregates tend to dissociate. At lower shear rates, the weaker shear forces allow these aggregates to remain intact, thereby maintaining a higher viscosity.

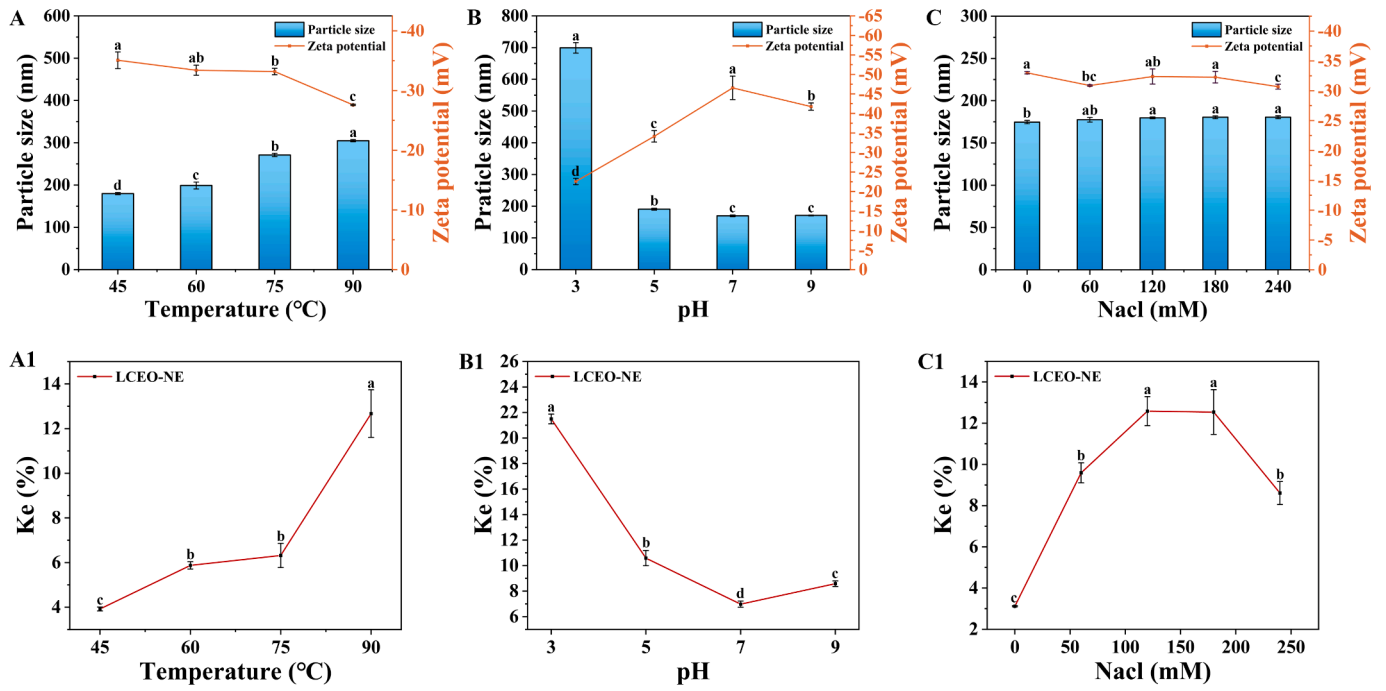

Fig. 3. Effect of temperature (A, A1), pH (B, B1), and salinity (C, C1) on LCEO-NE particle size, zeta potential, and Ke. Different lowercase letters indicate significant differences in particle size, zeta potential, or Ke ($p < 0.05$).

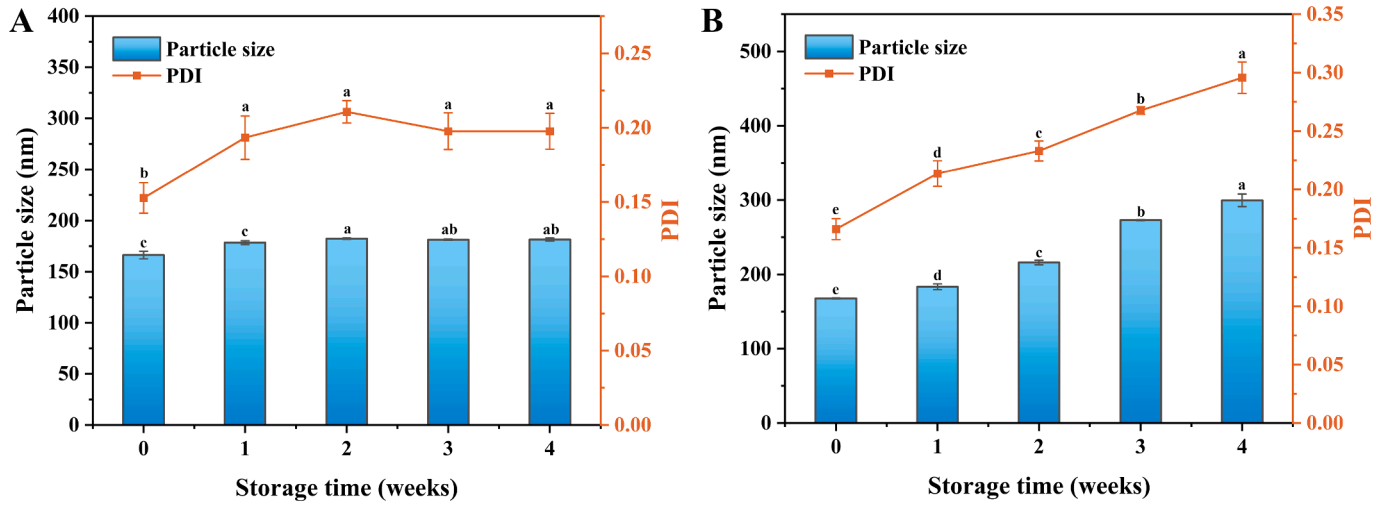

Fig. 4. Changes in particle size and PDI of LCEO-NE over four weeks of storage at 4 °C (A) and 25 °C (B). Different lowercase letters indicate significant differences in particle size or PDI ($p < 0.05$).

However, with increasing shear rates, the aggregates may not sustain their structure, leading to a substantial reduction in apparent viscosity [48]. Furthermore, at higher shear rates, the apparent viscosity tended towards near-zero values. This phenomenon is likely due to a dynamic equilibrium where the rate of floc breakdown equals their rate of formation, stabilizing the apparent viscosity at a very low-level [49]. Similar observations have been reported in a previous study [21].

3.5. Physicochemical stability measurements

3.5.1. Stability under different thermal treatment

From Fig. 3A and A1, it was evident that LCEO-NE experienced only minor fluctuations in particle size, ZP, and KE values within the temperature range of 45–75 °C, indicating relative stability. However, at 90 °C, a slight increase in particle size to 304.90 ± 2.66 nm was observed, accompanied by a decrease in the absolute ZP value to 27.58 ± 0.11 mV and a reduction in KE value. This suggests a marginal decline in stability, albeit the particle size remains around 300 nm even at such high temperatures, indicating the remarkable thermal stability of LCEO-NE.

3.5.2. Stability under different pH

Fig. 3B and B1, revealed that the properties of LCEO-NE were stable at pH levels of 5, 7, and 9. However, at pH 3, significant changes were noted: the particle size escalated to 699.37 ± 16.60 nm, the absolute ZP value diminished to below 22.58 ± 0.83 mV, and the KE value increased to 21.50 ± 0.38%. Similar phenomena have been documented in previous literature [11]. This may be because extremely low pH conditions can disrupt the structure of WP, diminishing its emulsifying efficacy and consequently, the stability of the nano-emulsion [50].

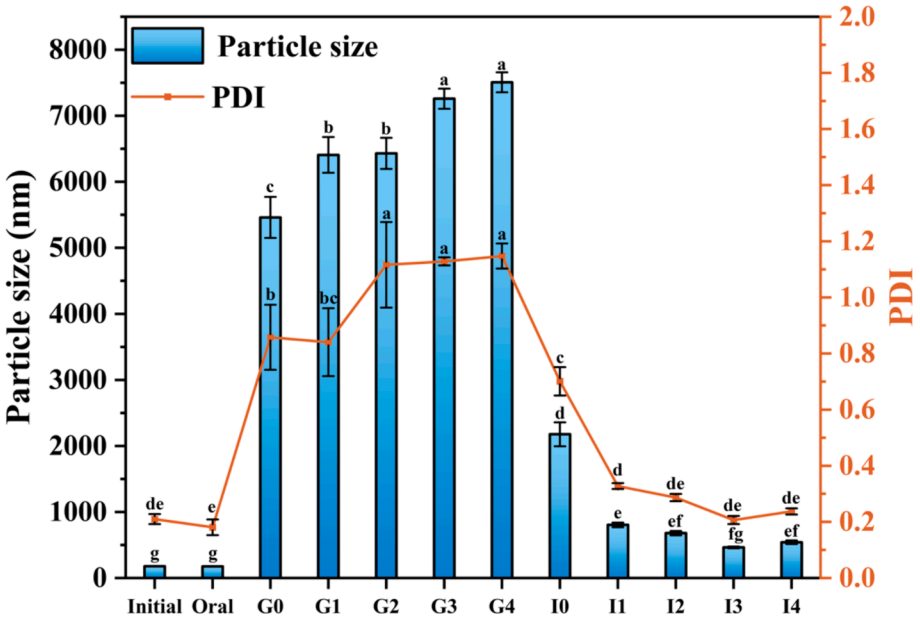

Fig. 5. G0, G1, G2, G3, G4 and I0, I1, I2, I3, I4 indicate the particle size and PDI of LCEO-NE after 0, 0.5, 1, 1.5, 2 h of digestion in the stomach and intestine, respectively. Different lowercase letters indicate significant differences in particle size or PDI ($p < 0.05$).

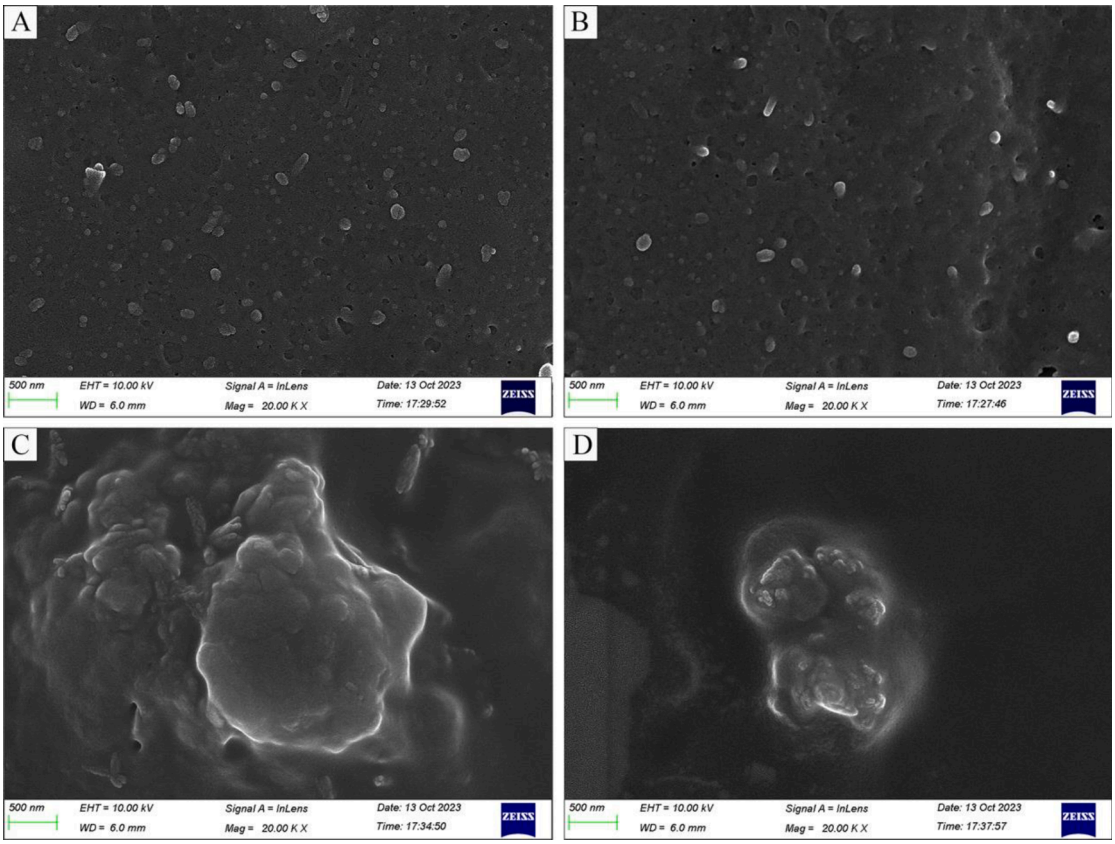

Fig. 6. Microstructure of LCEO-NE after *in vitro* digestion observed under SEM. A (initial), B (oral), C (gastric), D (intestine).

3.5.3. Stability under different salinity

From Fig. 3C and C1, variations in salinity had negligible effects on the particle size and ZP of LCEO-NE, with KE values consistently within 13%. This indicates a robust resistance to salt, which is advantageous for future processing and applications.

3.5.4. Determination of storage stability

In Fig. 4A, it was observed that the particle size and PDI of LCEO-NE remained stable below 185 nm and 0.2, respectively, after 4 weeks of storage at 4 °C. However, after the same storage period at 25 °C, the particle size and PDI increased to 299.53 ± 8.54 nm and 0.296 ± 0.013 (Fig. 4B), respectively. These findings indicate that LCEO-NE can be

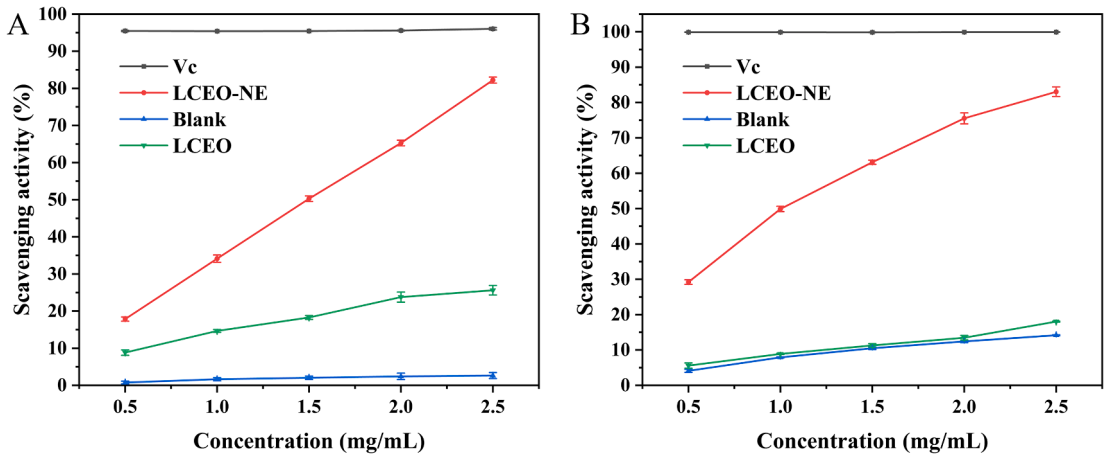

Fig. 7. *In vitro* antioxidant activities of LCEO-NE, LCEO, Blank, and Vc. (A) DPPH radical scavenging assay; (B) ABTS radical scavenging assay.

Table 2
The MIC and MBC of LCEO-NE, LCEO, Levofloxacin and WP.

Microorganisms	LCEO-NE (mg/mL)		LCEO (mg/mL)		Levofloxacin (μg/mL)		WP (mg/mL)	
	MIC	MBC	MIC	MBC	MIC	MBC	MIC	MBC
B. subtilis	0.125	0.25	0.25	1	0.048	0.096	> 32	> 32
E. coli	0.25	0.5	0.5	1	0.096	0.192	> 32	> 32
S. aureus	0.125	0.5	0.5	2	0.096	0.192	> 32	> 32
S. typhimurium	0.25	0.5	0.5	1	0.096	0.192	> 32	> 32
P. aeruginosa	0.5	1	1	1	0.048	0.096	> 32	> 32

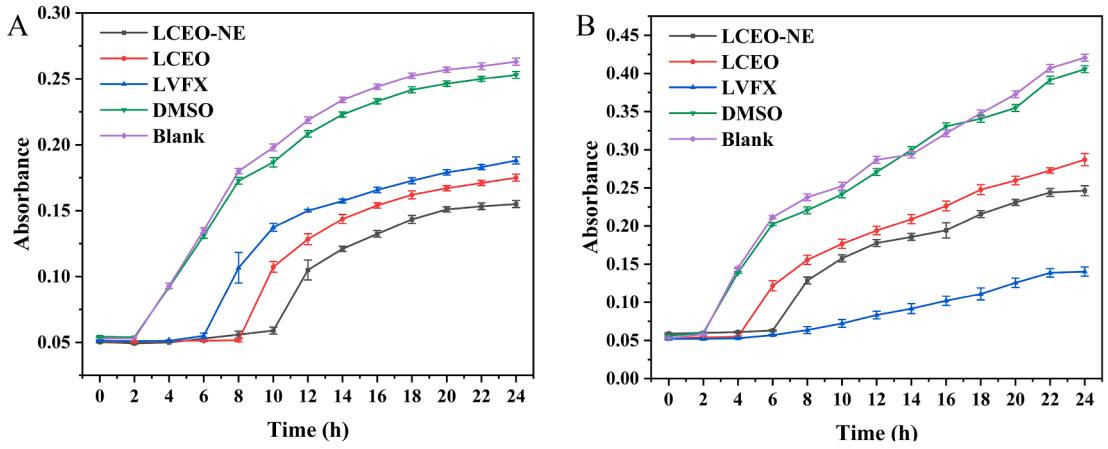

Fig. 8. Dynamic growth curves of bacteria treated with LCEO-NE, LCEO, LVFX, 2% DMSO, and Blank control. *E. coli* (A), *S. aureus* (B).

stored for longer periods at lower temperatures, with a slight decrease in stability at higher temperatures. This phenomenon might be attributed to the reduced thermodynamic motion of molecules at low temperatures, resulting in a lower frequency of molecular collisions. Consequently, this helps to maintain the steady state of the molecules and particles in the nano-emulsion, thereby prolonging the storage time [51]. A study by Carpenter et al. demonstrated that nano-emulsion prepared using an ultrasound-assisted method exhibited good storage stability over 12 weeks [52].

3.6. Effect of in vitro gastrointestinal digestion on LCEO-NE

3.6.1. Influence on particle size and PDI

As depicted in Fig. 5, LCEO-NE exhibited considerable stability during simulated oral digestion, with only minor changes in particle size (from 178.30 ± 2.63 nm to 175.73 ± 2.52 nm) and PDI (from 0.210 ± 0.018 to 0.181 ± 0.028) over 5 min. This stability is favorable for drug delivery applications. Conversely, significant changes in both particle size and PDI were observed during simulated gastrointestinal digestion. At the onset of the gastric phase, the particle size and PDI of LCEO-NE increased substantially, from 175.73 ± 2.52 nm to 5461.17 ± 310.80 nm, and from 0.181 ± 0.028 to 0.858 ± 0.116, respectively. These findings align with the observation in 3.5.2, where acidic conditions in the gastric juice altered the structural properties of the emulsifier, WP. Over the next 2 h, the particle size and PDI increased further to 7506.80 ± 151.32 nm and 1.147 ± 0.045, respectively. This is likely attributed to the presence of pepsin in the simulated gastric fluid, which disrupts the structure of the nano-emulsion, leading to the formation of a larger aggregate [53]. These findings are consistent with a previous study [54].

At the beginning of the intestinal digestion phase, a marked reduction in both particle size and PDI of LCEO-NE was observed, from 7506.80 ± 151.32 nm and 1.147 ± 0.045 to 2176.37 ± 180.55 nm and

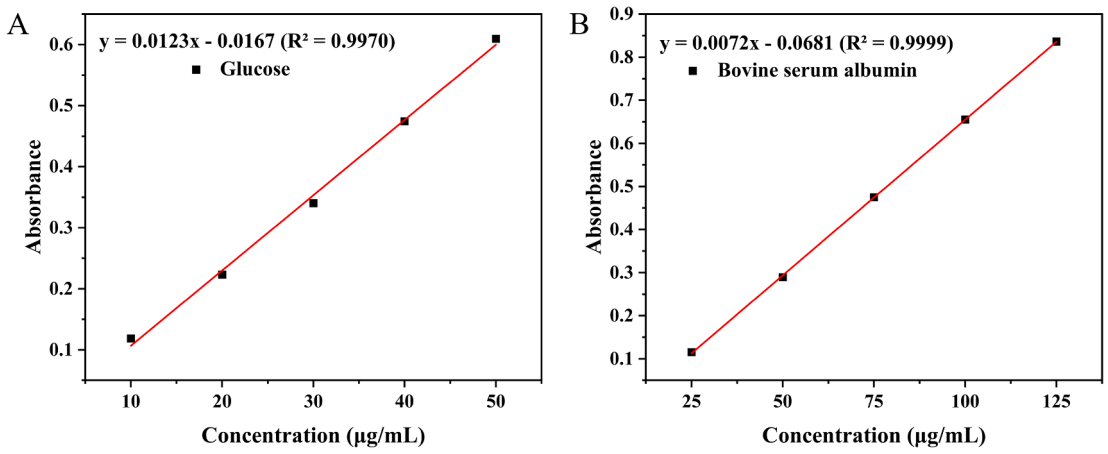

Fig. 9. Standard curves for glucose (A) and BSA (B).

Table 3
Extracellular nucleic acids absorbance, extracellular polysaccharides content, and extracellular soluble proteins content of bacteria after LCEO-NE, LCEO, 2% DMSO, and Blank control treatment.

Samples	extracellular nucleic acids		extracellular polysaccharides (μg/mL)		extracellular soluble proteins (μg/mL)	
	S. aureus	*E. coli*	*S. aureus*	*E. coli*	*S. aureus*	*E. coli*
LCEO-NE	2.5703 ± 0.0018^{a}	2.2300 ± 0.0028^{a}	93.77 ± 0.34^{a}	106.26 ± 0.46^{a}	87.23 ± 0.49^{a}	74.80 ± 1.36^{a}
LCEO	2.4928 ± 0.0032^{b}	1.9049 ± 0.0059^{b}	74.03 ± 1.14^{b}	83.58 ± 0.42^{b}	53.38 ± 0.65^{b}	48.84 ± 0.24^{b}
2% DMSO	0.0289 ± 0.0027^{c}	0.0263 ± 0.0003^{c}	9.28 ± 0.05^{d}	7.60 ± 0.05^{d}	13.88 ± 0.10^{c}	13.74 ± 0.26^{c}
Blank	0.0122 ± 0.0006^{d}	0.0016 ± 0.0004^{d}	23.47 ± 0.14^{c}	22.02 ± 0.15^{c}	12.75 ± 0.11^{d}	14.60 ± 0.11^{c}

Values mean ± SD; n = 3. Different letters in the same column indicate significant differences ($p < 0.05$).

Table 4
The IC_{50} of LCEO and LCEO-NE in scavenging DPPH and ABTS free radicals.

Samples	DPPH (mg/mL)	ABTS (mg/mL)
LCEO	13.597 ± 3.083	34.186 ± 3.063
LCEO-NE	1.590 ± 0.013	0.959 ± 0.019

Values mean ± SD; n = 3. The IC_{50} value represents the concentration at which 50 % inhibition of DPPH and ABTS radicals is achieved.

0.701 ± 0.0505, respectively. This reduction may be due to the transition of LCEO-NE from the SGF (pH 2) to the neutral environment of SIF (pH 7), enabling WP to partially regain their structure and redisperse aggregated components in LCEO-NE [55]. Over the subsequent 2 h, particle size and PDI further decreased to 541.63 ± 28.55 nm and 0.237 ± 0.011, respectively, likely because pancreatic lipase breaks down the LCEO in the aggregates formed during gastric digestion into free fatty acids and glycerol, consequently, new micelles and vesicles form, stabilizing the emulsions during the intestine phase [56]. A similar observation was reported in a study on the *in vitro* intestinal digestion of curcumin nano-emulsion [57].

3.6.2. Influence on microstructure

The microstructural changes of LCEO-NE post-simulated digestion were depicted in Fig. 6A–D, SEM images revealed that LCEO-NE maintained its morphology in the oral environment, indicating that saliva does not disrupt its morphology. However, after gastric digestion, LCEO-NE aggregated into larger-size agglomerates. At the end of intestinal digestion, these agglomerates were broken down into smaller agglomerates, thus confirming the particle size changes observed in 3.6.1.

3.7. Antioxidant activity analysis

3.7.1. Scavenging of DPPH radicals

As can be seen in Fig. 7A, LCEO-NE showed strong scavenging activity against DPPH radicals with an IC_{50} value of 1.590 ± 0.013 mg/mL, which was significantly smaller than that of LCEO (13.597 ± 3.083 mg/mL) (Table 4). The maximum scavenging rate of LCEO-NE and LCEO observed within the experimental concentration range was 82.24% ± 0.825% and 25.62% ± 1.28%, respectively. Notably, the scavenging rate of LCEO-NE significantly surpassed that of LCEO. This enhanced activity may be attributed to two factors: Firstly, the nano-emulsion form improves the dispersion and solubility of WP and LCEO in the aqueous phase, preventing aggregation of oil droplets and WP particles and thereby enhancing the stability of the entire system [58]. This stability facilitates more effective interactions with free radicals. Secondly, the smaller particle size of LCEO-NE results in a larger specific surface area, providing more reaction sites for interaction with free radicals, thereby boosting its scavenging capacity [59]. After being prepared into nano-emulsion, both Zanthoxylum bungeanum Maxim essential oil and clove essential oil showed enhanced DPPH scavenging ability, aligning with our findings [21,60].

3.7.2. Scavenging of ABTS radicals

Fig. 7B illustrated a positive correlation between concentration and ABTS radical scavenging efficiency for all samples. The scavenging rate of LCEO-NE reached 82.24 ± 0.825% at a concentration of 2.5 mg/mL. The IC_{50} values of LCEO and LCEO-NE were 0.959 ± 0.019 mg/mL and 34.186 ± 3.063 mg/mL (Table 4), respectively. These results indicate that the nano-emulsion formation significantly enhances the antioxidant capacity of LCEO. This enhancement is consistent with the observed DPPH radical scavenging rate and confirms the hypothesis in 3.7.1. In conclusion, LCEO-NE has a strong antioxidant capacity and can be used as a natural antioxidant in food and pharmaceuticals.

3.8. Antibacterial activity

3.8.1. Determination of minimum inhibitory concentration (MIC) and minimum bactericidal concentration (MBC)

The results of MIC and MBC were presented in Table 2, revealing that

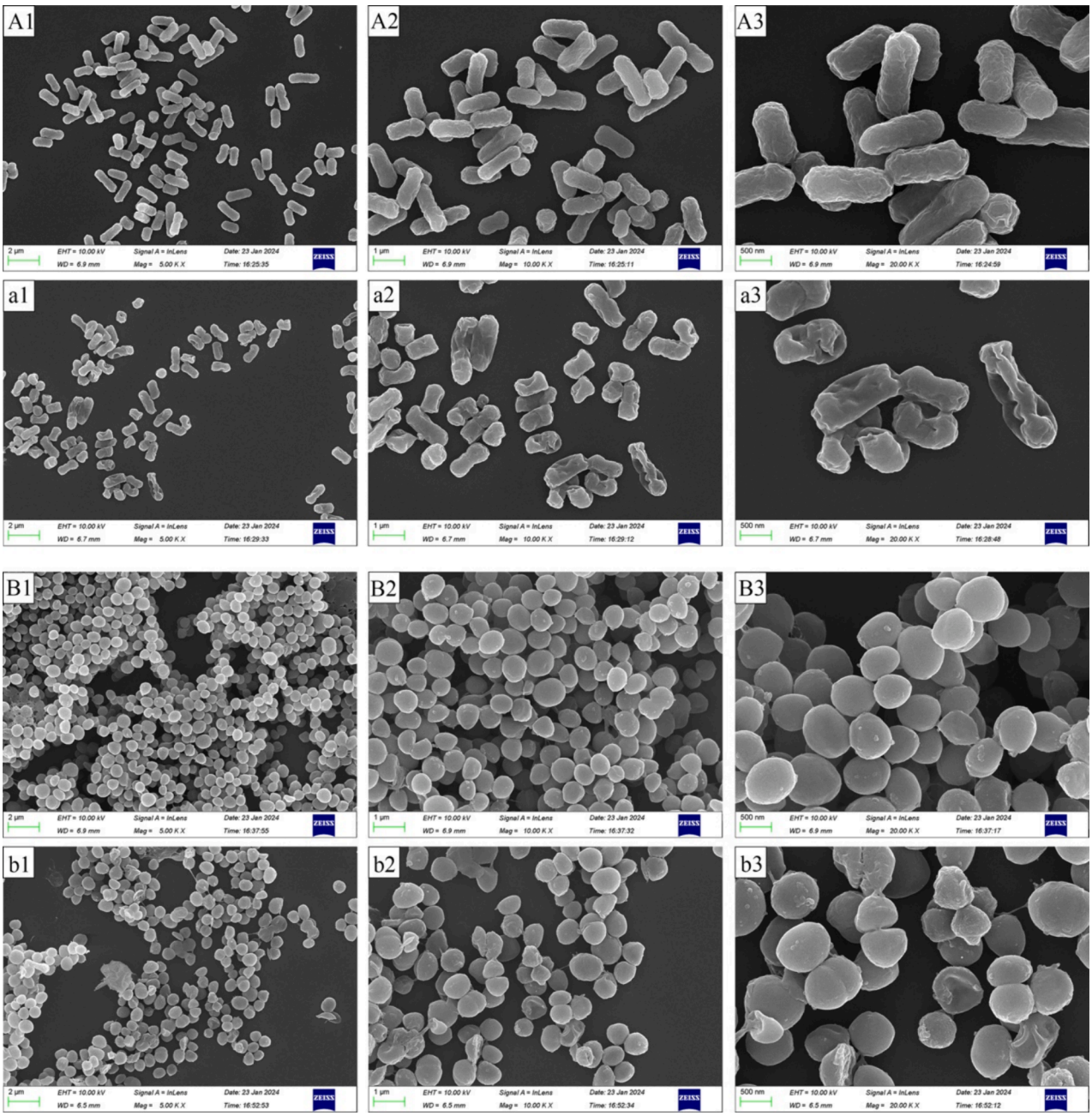

Fig. 10. Scanning electron microscopy images of *E. coli* and *S. aureus*. A1 (2 μm), A2 (1 μm), A3 (500 nm) and B1 (2 μm), B2 (1 μm), B3 (500 nm) are untreated *E. coli* and *S. aureus*, respectively; a1 (2 μm), a2 (1 μm), a3 (500 nm) and b1 (2 μm), b2 (1 μm), b3 (500 nm) are LCEO-NE-treated *E. coli* and *S. aureus*, respectively.

WP did not exhibit inhibitory effects on any of the tested bacteria at concentrations up to 32 mg/mL. In contrast, both LCEO-NE and LCEO displayed significant inhibitory effects. Notably, LCEO-NE demonstrated lower MIC and MBC values than LCEO for all tested bacteria, indicating its superior antimicrobial efficacy. This enhanced action of LCEO-NE may be attributed to its smaller size, facilitating more efficient penetration through biological membranes, enabling the antimicrobial agent in LCEO-NE to access and disrupt the physiological structure of the bacteria more effectively [61]. Additionally, the reduced size of the oil droplets in the nano-emulsion increases the surface area for interaction with bacterial cells, potentially enhancing the antimicrobial effectiveness. Furthermore, LCEO-NE exhibited lower MIC and MBC values against Gram-positive bacteria (*B. subtilis* and *S. aureus*) compared to Gram-negative bacteria (*E. coli*, *S. typhimurium*, and *P. aeruginosa*), indicating a higher susceptibility of Gram-positive bacteria to LCEO-NE. These findings align with a previous study demonstrating that Gram-negative bacteria tend to exhibit higher resistance to cinnamon essential oil compared to Gram-positive bacteria [9].

3.8.2. Determination of bacterial growth curves

The bacterial growth curves help to understand the bacteriostatic potency of the samples [62]. As depicted in Fig. 8A and B, *S. aureus* and *E. coli* began to grow after 8 h and 4 h respectively following LCEO treatment, continuing at a slow pace thereafter. However, after treatment with LCEO-NE, these bacteria initiated growth at 10 h and 6 h respectively and ceased growing at 20 h and 22 h respectively, with significantly weaker growth trends compared to the LCEO-treated group. This suggests that both LCEO-NE and LCEO exerted inhibitory effects on *S. aureus* and *E. coli*, with the inhibitory effect of LCEO-NE being stronger and more durable. Additionally, the growth of *S. aureus*

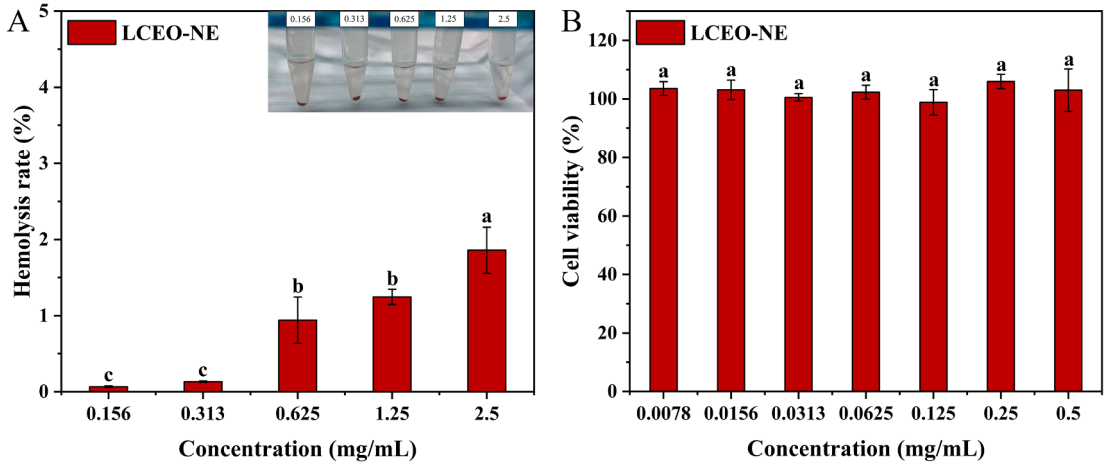

Fig. 11. Hemolysis percentages of LCEO-NE (A); Effects of LCEO-NE on the viability of L02 cells (B). Different lowercase letters represent significant differences between Hemolysis rate or cell viability ($p < 0.05$).

commenced later than that of *E. coli* following treatment with LCEO-NE, indicating that LCEO-NE is more sensitive to Gram-positive bacteria.

3.8.3. Antibacterial mechanism

3.8.3.1. Extracellular nucleic acids absorbance, polysaccharides content, and soluble proteins content of bacteria. Nucleic acids, encompassing DNA and RNA, are fundamental in bacterial cells, orchestrating genetic information flow, biosynthesis, and metabolic pathways [63]. Proteins, integral to bacterial vitality, are involved in maintaining cellular structure, signaling, metabolic regulation, and immune responses. They act as channels or receptors on cell membranes, modulating substance movement, and mediating extracellular interactions with hosts [64]. Polysaccharides, constituting the peptidoglycan layer of cell walls, provide structural integrity and protection, enabling bacteria to withstand various environmental stresses [65]. The collaborative interaction of these biomolecules equips bacteria with the versatility to adapt to diverse environments and maintain essential biological functions. Monitoring the extracellular alterations in these biomolecules can be instrumental in identifying specific structural damages in bacteria.

The standard curves for glucose and BSA were represented by $y = 0.0123x - 0.0167$ ($R^2 = 0.9970$) (Fig. 9A) and $y = 0.0072x - 0.0681$ ($R^2 = 0.9999$) (Fig. 9B), respectively, showing high linearity. As presented in Table 3, the contents of extracellular nucleic acids, extracellular polysaccharides, and extracellular soluble proteins in the LCEO-NE-treated bacteria were higher than those in the LCEO-treated group and significantly higher than those in the blank control group. These findings suggest that the antibacterial mechanisms of LCEO-NE and LCEO are similar, with the former being more effective, primarily characterized by the destruction of the cell membrane and cell wall, resulting in the efflux of cell contents and ultimately leading to the death of bacterial cells.

3.8.3.2. Bacterial ultrastructure. Normal *E. coli* exhibited short, rod-like structures with regular morphology (Fig. 10A1–A3). In contrast, *E. coli* treated with LCEO-NE showed significant morphological alterations, including crumpling, severe inward depressions, irregular shapes, and in some instances, broken and incomplete structures (Fig. 10a1–a3). Similarly, typical spherical structures with smooth surfaces were observed in normal *S. aureus* (Fig. 10B1–B3), while LCEO-NE-treated *S. aureus* displayed wrinkling and shriveling (Fig. 10b1–10b3). These observations confirm the above hypothesis about the antimicrobial mechanism of LCEO-NE.

3.9. Security assessment

3.9.1. Hemocompatibility test

Hemocompatibility is a critical parameter for assessing biocompatibility [66]. As depicted in Fig. 11A, the hemolysis rate of LCEO-NE increased with the concentration of the nano-emulsion, which was almost equal to 0 at a concentration of 1 mg/mL, even when the concentration increased to 2.5 mg/mL, it around 2%. Previous literature indicated that a hemolysis rate of less than 5% was considered safe and non-hemolytic [67]. The above results demonstrate that LCEO-NE exhibits excellent biosafety and holds promising potential for applications in drug transportation.

3.9.2. Determination of cytotoxicity

Cytotoxicity serves as a pivotal indicator for assessing the safety of a formulation, with higher cell survival rates indicating lower cytotoxicity of the formulation. The effect of LCEO-NE on the cell viability of L02 was evaluated by CCK-8 assay. The results showed that the viability of L02 cells remained above 98% after treatment with LCEO-NE (0.0078–0.5 mg/mL), and the cell viability exceeded 100% at concentrations of 0.25 mg/mL and 0.5 mg/mL (Fig. 11B). This anomaly may be attributed to the nutritional properties of LCEO-NE, which have the potential to enhance cellular energy supply and promote cell proliferation. Therefore, LCEO-NE was not toxic to normal human hepatocytes in this concentration range and showed good biocompatibility. Similarly, nano-emulsion encapsulated sea buckthorn fruit oil did not inhibit cell proliferation [11].

4. Conclusion

A new green LCEO-NE was successfully prepared by ultrasound-assisted technique with extremely low energy consumption. It was characterized by a spherical shape, small average particle size, and uniform distribution. This novel formulation exhibited enhanced stability, safety, antioxidant activity, and antimicrobial properties compared to raw LCEO. *In vitro* digestion test indicated it remained stable in the oral phase then digested and decomposed in the gastrointestinal tract environment. Moreover, LCEO-NE demonstrated potent inhibitory effects against all five tested bacterial strains, particularly Gram-positive bacteria. The inhibitory mechanism involved damaging the bacterial cell membrane and cell wall, leading to the leakage of bacterial contents and subsequent bacterial death. Hemolysis and cytotoxicity experiments confirmed the high safety profile of LCEO-NE. In summary, nano-emulsion represents an effective packaging strategy to enhance the stability, bioactivity, and safety of LCEO. These findings

provide a theoretical foundation for applying Litsea cubeba essential oil in the healthcare, pharmaceutical, and environment industries.

CRediT authorship contribution statement

Qiang Peng: Writing – review & editing, Writing – original draft, Software, Data curation, Conceptualization. **Zhiwu Huang:** Investigation, Formal analysis. **Guixin Liang:** Methodology, Formal analysis. **Yongguang Bi:** Project administration, Funding acquisition, Conceptualization. **Fansheng Kong:** Validation, Formal analysis. **Zhong Wang:** Validation, Formal analysis. **Shaofan Tan:** Validation, Formal analysis. **Junyong Zhang:** Writing – review & editing.

Declaration of competing interest

The authors declare that they have no known competing financial interests or personal relationships that could have appeared to influence the work reported in this paper.

Acknowledgments

This work is financially supported by Yunfu Traditional Chinese Medicine (Southern Medicine) Innovation Team Project, Guangdong Provincial Doctoral Workstation [No. 2020-216(192)], Science and Technology Planning Project of Guangzhou Science and Technology Bureau (No. 202102080365), Yunfu City Science and Technology Plan Project (No. 2020020101), Science and Technology Planning Project of Guangdong Science and Technology Department (No. KTP20200170), Project of Traditional Chinese Medicine Bureau of Guangdong Province (No. 20231422), Zhongshan Social Welfare and Basic Research Program (No. 2020B2005), Project of Guangdong Provincial Department of Education - special projects in key areas (No. 2021ZDZX4013), Heyuan City Science and Technology Plan Project (No. 2018014) and Guangdong MEPP Fund (No. GDOE[2019]A27).

References

[1] R. Ni, P. Wang, P. Zhan, H. Tian, T. Li, Effects of different frying temperatures on the aroma profiles of fried mountain pepper (Litsea cubeba (Lour.) Pers.) oils and characterization of their key odorants, Food Chem. 357 (2021) 129786, https://doi.org/10.1016/j.foodchem.2021.129786.
[2] Y. Zhao, Y. Chen, M. Gao, L. Wu, Y. Wang, Comparative investigation of key aroma terpenoids of Litsea cubeba essential oil by sensory, chromatographic, spectral and molecular studies, LWT 176 (2023) 114519, https://doi.org/10.1016/j.lwt.2023.114519.
[3] Y.-S. Wang, Z.-Q. Wen, B.-T. Li, H.-B. Zhang, J.-H. Yang, Ethnobotany, phytochemistry, and pharmacology of the genus Litsea: An update, J. Ethnopharmacol. 181 (2016) 66–107, https://doi.org/10.1016/j.jep.2016.01.032.
[4] D.-G. Kong, Y. Zhao, G.-H. Li, B.-J. Chen, X.-N. Wang, H.-L. Zhou, H.-X. Lou, D.-M. Ren, T. Shen, The genus Litsea in traditional Chinese medicine: An ethnomedical, phytochemical and pharmacological review, J. Ethnopharmacol. 164 (2015) 256–264, https://doi.org/10.1016/j.jep.2015.02.020.
[5] K. Liu, X. Xu, H. Liu, Z. Liu, K. Zhao, Y. Ma, K. Zhang, Mechanical properties and water sensitivity of soybean protein isolate film improved by incorporation of sodium caseinate and transglutaminase, Prog. Org. Coat. 153 (2021) 106154, https://doi.org/10.1016/j.porgcoat.2021.106154.
[6] A. Mushtaq, S. Mohd Wani, A.R. Malik, A. Gull, S. Ramniwas, G. Ahmad Nayik, S. Ercisli, R. Alina Marc, R. Ullah, A. Bari, Recent insights into Nanoemulsions: Their preparation, properties and applications, Food Chemistry: X 18 (2023) 100684, https://doi.org/10.1016/j.fochx.2023.100684.
[7] S. Christaki, T. Moschakis, M. Hatzikamari, I. Mourtzinos, Nanoemulsions of oregano essential oil and green extracts: Characterization and application in whey cheese, Food Control 141 (2022) 109190, https://doi.org/10.1016/j.foodcont.2022.109190.
[8] S. Garzoli, S. Petralito, E. Ovidi, G. Turchetti, V. Laghezza Masci, A. Tiezzi, J. Trilli, S. Cesa, M.A. Casadei, P. Giacomello, P. Paolicelli, Lavandula x intermedia essential oil and hydrolate: Evaluation of chemical composition and antibacterial activity before and after formulation in nanoemulsion, Ind. Crop. Prod. 145 (2020) 112068, https://doi.org/10.1016/j.indcrop.2019.112068.
[9] D. Liang, B. Feng, N. Li, L. Su, Z. Wang, F. Kong, Y. Bi, Preparation, characterization, and biological activity of Cinnamomum cassia essential oil nanoemulsion, Ultrason. Sonochem. 86 (2022) 106009, https://doi.org/10.1016/j.ultsonch.2022.106009.
[10] R. Adjonu, G. Doran, P. Torley, S. Agboola, Whey protein peptides as components of nanoemulsions: A review of emulsifying and biological functionalities, J. Food Eng. 122 (2014) 15–27, https://doi.org/10.1016/j.jfoodeng.2013.08.034.
[11] Q. Zhang, C. Zhang, X. Luo, Z. Wang, J. Guo, Y. Bi, Protein stabilized seabuckthorn fruit oil nanoemulsion:Preparation, characterization and performance research, Food Biosci. 46 (2022) 101597, https://doi.org/10.1016/j.fbio.2022.101597.
[12] T. Jiang, W. Liao, C. Charcosset, Recent advances in encapsulation of curcumin in nanoemulsions: A review of encapsulation technologies, bioaccessibility and applications, Food Res. Int. 132 (2020) 109035, https://doi.org/10.1016/j.foodres.2020.109035.
[13] S.M.M. Modarres-Gheisari, R. Gavagsaz-Ghoachani, M. Malaki, P. Safarpour, M. Zandi, Ultrasonic nano-emulsification – A review, Ultrason. Sonochem. 52 (2019) 88–105, https://doi.org/10.1016/j.ultsonch.2018.11.005.
[14] H. Schestkowa, T. Wollborn, A. Westphal, A. Maria Wagemans, U. Fritsching, S. Drusch, Conformational state and charge determine the interfacial stabilization process of beta-lactoglobulin at preoccupied interfaces, J. Colloid Interface Sci. 536 (2019) 300–309, https://doi.org/10.1016/j.jcis.2018.10.043.
[15] S. Calligaris, S. Plazzotta, F. Bot, S. Grasselli, A. Malchiodi, M. Anese, Nanoemulsion preparation by combining high pressure homogenization and high power ultrasound at low energy densities, Food Res. Int. 83 (2016) 25–30, https://doi.org/10.1016/j.foodres.2016.01.033.
[16] G. Fan, X. Ning, S. Chen, L. Zhong, C. Guo, Y. Yang, J. Liu, M. Tang, G. Liao, X. Wang, Z. Wang, J. Wang, Differences in fruit yields and essential oil contents and composition among natural provenances of Litsea cubeba in China and their relationships with main habitat factors, Ind. Crop. Prod. 194 (2023) 116285, https://doi.org/10.1016/j.indcrop.2023.116285.
[17] G. Ghoshal, Shivani, Thyme essential oil nano-emulsion/Tamarind starch/Whey protein concentrate novel edible films for tomato packaging, Food Control 138 (2022) 108990, https://doi.org/10.1016/j.foodcont.2022.108990.
[18] L. Bai, S. Geng, Y. Zhou, H. Ma, B. Liu, Ultrasound-assisted fabrication and stability evaluation of okra seed protein stabilized nanoemulsion, Ultrason. Sonochem. 104 (2024) 106807, https://doi.org/10.1016/j.ultsonch.2024.106807.
[19] L. Zeng, Q. Peng, Q. Li, Y. Bi, F. Kong, Z. Wang, S. Tan, Synthesis, characterization, biological activity, and in vitro digestion of selenium nanoparticles stabilized by Antarctic ice microalgae polypeptide, Bioorg. Chem. 141 (2023) 106884, https://doi.org/10.1016/j.bioorg.2023.106884.
[20] W. Zhong, D. Li, L. Li, S. Yu, J. Pang, Z. Zhi, C. Wu, pH-responsive Pickering emulsion containing citrus essential oil stabilized by zwitterionically charged chitin nanofibers: Physicochemical properties and antimicrobial activity, Food Chem. 433 (2024) 137388, https://doi.org/10.1016/j.foodchem.2023.137388.
[21] Q. Li, Z. Chen, L. Zeng, Y. Bi, F. Kong, Z. Wang, S. Tan, Characterization, in-vitro digestion, antioxidant, anti-hyperlipidemic and antibacterial activities of Zanthoxylum bungeanum Maxim essential oil nano-emulsion, Food Biosci. 56 (2023) 103082, https://doi.org/10.1016/j.fbio.2023.103082.
[22] Y. Shi, M. Zhang, K. Chen, M. Wang, Nano-emulsion prepared by high pressure homogenization method as a good carrier for Sichuan pepper essential oil: Preparation, stability, and bioactivity, LWT 154 (2022) 112779, https://doi.org/10.1016/j.lwt.2021.112779.
[23] M. Hamdi, H. Mostafa, M. Aldhaheri, P. Mudgil, H. Kamal, A.S. Alamri, C. M. Galanakis, S. Maqsood, Valorization of different low-grade date (Phoenix dactylifera L.) fruit varieties: A study on the bioactive properties of polyphenolic extracts and their stability upon in vitro simulated gastrointestinal digestion, Plant Physiol. Biochem. 200 (2023) 107764, https://doi.org/10.1016/j.plaphy.2023.107764.
[24] S.F. Sadeghian, M. Majdinasab, M. Nejadmansouri, S.M.H. Hosseini, Effects of natural antioxidants and high-energy fabrication methods on physical properties and oxidative stability of flaxseed oil-in-water nanoemulsions, Ultrason. Sonochem. 92 (2023) 106277, https://doi.org/10.1016/j.ultsonch.2022.106277.
[25] S. Sihag, A. Pal, Ravikant, V. Saharan, Antioxidant properties and free radicals scavenging activities of pomegranate (Punica granatum L.) peels: An in-vitro study, Biocatal. Agric. Biotechnol. 42 (2022) 102368, https://doi.org/10.1016/j.bcab.2022.102368.
[26] L.T. Cardoso, B. Alexandre, F.A. Cacciatore, Y.V.d.S. Magedans, A.G. Fett-Neto, R. V. Contri, P.d.S. Malheiros, Carvacrol-loaded nanoemulsions produced with a natural emulsifier for lettuce sanitization, Food Res. Int. 168 (2023) 112748, https://doi.org/10.1016/j.foodres.2023.112748.
[27] S.A. Al Yousef, In vitro bactericidal and imipenem synergistic effect of nano-silver against multiple drug-resistant Pseudomonas aeruginosa, Journal of King Saud University - Science 34 (2022) 101706, https://doi.org/10.1016/j.jksus.2021.101706.
[28] R. He, H. Chen, H. Wu, J. Liu, W. Chen, M. Zhang, W. Chen, Q. Zhong, Proteomics reveals energy limitation and amino acid consumption as antibacterial mechanism of linalool against Shigella sonnei and its application in fresh beef preservation, Food Chemistry: X 19 (2023) 100837, https://doi.org/10.1016/j.fochx.2023.100837.
[29] L. Tang, X. Luo, M. Wang, Z. Wang, J. Guo, F. Kong, Y. Bi, Synthesis, characterization, in vitro antioxidant and hypoglycemic activities of selenium nanoparticles decorated with polysaccharides of Gracilaria lemaneiformis, Int. J. Biol. Macromol. 193 (2021) 923–932, https://doi.org/10.1016/j.ijbiomac.2021.10.189.
[30] Y.-S. Li, Y.-S. Ge, Y. Zhang, A.-Q. Zhang, S.-F. Sun, F.-L. Jiang, Y. Liu, Interaction of coomassie brilliant blue G250 with human serum albumin: Probing of the binding mechanism and binding site by spectroscopic and molecular modeling methods, J. Mol. Struct. 968 (2010) 24–31, https://doi.org/10.1016/j.molstruc.2010.01.015.

[31] D. Mishra, P. Khare, D.K. Singh, V. Yadav, S. Luqman, P.V.A. Kumar, K. Shanker, Synthesis of Ocimum extract encapsulated cellulose nanofiber/chitosan composite for improved antioxidant and antibacterial activities, Carbohydr. Polym. Technol. Appl. 2 (2021) 100152, https://doi.org/10.1016/j.carpta.2021.100152.
[32] H. Sun, H. Zheng, Z. Zhang, Y. Liu, J. Qu, X. Zhu, Cytotoxicity assessment of nanoplastics and associated additives using an electrochemical sensor based on carbon nanohorn/gold nanoparticles, J. Environ. Chem. Eng. 11 (2023) 111452, https://doi.org/10.1016/j.jece.2023.111452.
[33] C. Bailly, Targets and pathways involved in the antitumor activity of citral and its stereo-isomers, Eur. J. Pharmacol. 871 (2020) 172945, https://doi.org/10.1016/j.ejphar.2020.172945.
[34] G.-R. Adriana Estrella, G.-T. María Eva, H.-L. Alberto, V.-D. María Guadalupe, C.-V. Azucena, O.-S. Sandra, A.-V. Noé, L.-M. Francisco Javier, Limonene from Agastache mexicana essential oil produces antinociceptive effects, gastrointestinal protection and improves experimental ulcerative colitis, J. Ethnopharmacol. 280 (2021) 114462, https://doi.org/10.1016/j.jep.2021.114462.
[35] M. Allenspach, C. Steuer, α-Pinene: A never-ending story, Phytochemistry 190 (2021) 112857, https://doi.org/10.1016/j.phytochem.2021.112857.
[36] F.R. Pinheiro-Neto, E.M. Lopes, B.T. Acha, L.d.S. Gomes, W.A. Dias, A.C.d. Reis Filho, B.d.S. Leal, D.C.d.N. Rodrigues, J.d.N. Silva, D. Dittz, P.M.P. Ferreira, F.R.d. C. Almeida, α-Phellandrene exhibits antinociceptive and tumor-reducing effects in a mouse model of oncologic pain, Toxicol. Appl. Pharmacol. 418 (2021) 115497, https://doi.org/10.1016/j.taap.2021.115497.
[37] L. Yu, Y. Zhou, Y. Chen, Y. Wang, Q. Gu, D. Song, Antifungal activity and mechanism of Litsea cubeba (Lour.) Persoon essential oil against the waxberry spoilage fungi Penicillium oxalicum and its potential application, Int. J. Food Microbiol. 411 (2024) 110512, https://doi.org/10.1016/j.ijfoodmicro.2023.110512.
[38] J. Huang, S. Liu, R. Liu, Y. Yi, C. Li, Z. Xiao, J. Tu, J. Xiao, Mechanisms of Litsea cubeba essential oil in the control of Colletotrichum scovillei in pepper (Capsicum annuum L.): Cell membrane/wall perspective, Physiol. Mol. Plant Pathol. 127 (2023) 102103, https://doi.org/10.1016/j.pmpp.2023.102103.
[39] M. Marhamati, G. Ranjbar, M. Rezaie, Effects of emulsifiers on the physicochemical stability of oil-in-water nanoemulsions: A critical review, J. Mol. Liq. 340 (2021) 117218, https://doi.org/10.1016/j.molliq.2021.117218.
[40] R. Song, Y. Lin, Z. Li, Ultrasonic-assisted preparation of eucalyptus oil nanoemulsion: Process optimization, in vitro digestive stability, and anti-Escherichia coli activity, Ultrason. Sonochem. 82 (2022) 105904, https://doi.org/10.1016/j.ultsonch.2021.105904.
[41] S.M.T. Gharibzahedi, S.M. Jafari, Chapter 9 - Fabrication of Nanoemulsions by Ultrasonication, in: S.M. Jafari, D.J. McClements (Eds.), Nanoemulsions, Academic Press, 2018, pp. 233–285, https://doi.org/10.1016/B978-0-12-811838-2.00009-6.
[42] Q. Ye, S. Kwon, Z. Gu, C. Selomulya, Stable nanoemulsions for poorly soluble curcumin: From production to digestion response in vitro, J. Mol. Liq. (2023) 123720, https://doi.org/10.1016/j.molliq.2023.123720.
[43] M. Lu, T. Zhang, Z. Jiang, Y. Guo, F. Qiu, R. Liu, L. Zhang, M. Chang, R. Liu, Q. Jin, X. Wang, Physical properties and cellular antioxidant activity of vegetable oil emulsions with different chain lengths and saturation of triglycerides, LWT 121 (2020) 108948, https://doi.org/10.1016/j.lwt.2019.108948.
[44] J. Loncke, A. Vancleef, W. Dermaut, L. Braeken, L.C.J. Thomassen, Development and characterization of a continuous ultrasound emulsification and nano-emulsion polymerization process, Tetrahedron Green Chem 2 (2023) 100023, https://doi.org/10.1016/j.tgchem.2023.100023.
[45] A. Kaushik, D. Joshi, R. Kumar Saw, K. Bala Rathi, S. Mitra, A. Mandal, Formation and characterization of nanoparticle assisted surfactant stabilized oil-in-water nanoemulsions for application in enhanced oil recovery, Fuel 359 (2024) 130500, https://doi.org/10.1016/j.fuel.2023.130500.
[46] S. Zhang, Q. Zhang, J. Shang, Z.-S. Mao, C. Yang, Measurement methods of particle size distribution in emulsion polymerization, Chin. J. Chem. Eng. 39 (2021) 1–15, https://doi.org/10.1016/j.cjche.2021.03.007.
[47] J.M. Stubbs, D.C. Sundberg, A round robin study for the characterization of latex particle morphology—multiple analytical techniques to probe specific structural features, Polymer 46 (2005) 1125–1138, https://doi.org/10.1016/j.polymer.2004.11.079.
[48] S. Tamnak, H. Mirhosseini, C.P. Tan, B. Tabatabaee Amid, M. Kazemi, S. Hedayatnia, Encapsulation properties, release behavior and physicochemical characteristics of water-in-oil-in-water (W/O/W) emulsion stabilized with pectin–pea protein isolate conjugate and Tween 80, Food Hydrocoll. 61 (2016) 599–608, https://doi.org/10.1016/j.foodhyd.2016.06.023.
[49] T. Yao, Y. Wen, Z. Xu, M. Ma, P. Li, C. Brennan, Z. Sui, H. Corke, Octenylsuccinylation differentially modifies the physicochemical properties and digestibility of small granule starches, Int. J. Biol. Macromol. 144 (2020) 705–714, https://doi.org/10.1016/j.ijbiomac.2019.12.129.
[50] S.A. Onaizi, Effect of oil/water ratio on rheological behavior, droplet size, zeta potential, long-term stability, and acid-induced demulsification of crude oil/water nanoemulsions, J. Pet. Sci. Eng. 209 (2022) 109857, https://doi.org/10.1016/j.petrol.2021.109857.
[51] M. Chang, Y. Guo, Z. Jiang, L. Shi, T. Zhang, Y. Wang, M. Gong, T. Wang, R. Lin, R. Liu, Y. Wang, Q. Jin, X. Wang, Sea buckthorn pulp oil nanoemulsions fabricated by ultra-high pressure homogenization process: A promising carrier for nutraceutical, J. Food Eng. 287 (2020) 110129, https://doi.org/10.1016/j.jfoodeng.2020.110129.
[52] J. Carpenter, V.K. Saharan, Ultrasonic assisted formation and stability of mustard oil in water nanoemulsion: Effect of process parameters and their optimization, Ultrason. Sonochem. 35 (2017) 422–430, https://doi.org/10.1016/j.ultsonch.2016.10.021.
[53] A. Kheroufi, M.E. Brassesco, D.A. Campos, A. Mouzai, H. Boughellouta, M. E. Pintado, Whey protein-derived peptides: The impact of chicken pepsin hydrolysis upon whey proteins concentrate on their biological and technological properties, Int. Dairy J. 134 (2022) 105442, https://doi.org/10.1016/j.idairyj.2022.105442.
[54] D. Liang, C. Wang, X. Luo, Z. Wang, F. Kong, Y. Bi, Preparation, characterization and properties of cinnamon essential oil nano-emulsion formed by different emulsifiers, J. Drug Delivery Sci. Technol. 86 (2023) 104638, https://doi.org/10.1016/j.jddst.2023.104638.
[55] S.-J. Bing, Y.-Q. Li, G.-J. Sun, C.-Y. Wang, Y. Liang, D.-L. Hua, L. Chen, H.-Z. Mo, Effect of different acidic or alkaline environments on structural characteristics, functional and physicochemical properties of lentinus edodes protein, Process Biochem. 130 (2023) 15–25, https://doi.org/10.1016/j.procbio.2023.04.001.
[56] M.R. Infantes-Garcia, S.H.E. Verkempinck, F. Carriére, M.E. Hendrickx, T. Grauwet, Pre-duodenal lipid digestion of emulsions: Relevance, colloidal aspects and mechanistic insight, Food Res. Int. 168 (2023) 112785, https://doi.org/10.1016/j.foodres.2023.112785.
[57] H. Jin, L. Shang, Y. Xue, Y. Wan, C. Liu, Z. Fan, J. Xu, Q. Zhao, Lipolytic behavior and bioaccessibility of curcumin nanoemulsions stabilized by rice bran protein hydrolysate, LWT 179 (2023) 114616, https://doi.org/10.1016/j.lwt.2023.114616.
[58] J.-L. He, B.-H. Liu, H.-L. Zhang, D. Xu, B.-M. Shi, Y.-H. Zhang, Improvement of hydrolysis efficiency and interfacial properties of zein using nanoemulsions prepared by a low energy emulsification method, Food Biosci. 54 (2023) 102922, https://doi.org/10.1016/j.fbio.2023.102922.
[59] A. Rehman, T. Qunyi, H.R. Sharif, S.A. Korma, A. Karim, M.F. Manzoor, A. Mehmood, M.W. Iqbal, H. Raza, A. Ali, T. Mehmood, Biopolymer based nanoemulsion delivery system: An effective approach to boost the antioxidant potential of essential oil in food products, Carbohydr. Polym. Technol. Appl. 2 (2021) 100082, https://doi.org/10.1016/j.carpta.2021.100082.
[60] A. Jindal, A. Kumar, Physical characterization of clove oil based self Nano-emulsifying formulations of cefpodoxime proxetil: Assessment of dissolution rate, antioxidant & antibacterial activity, OpenNano 8 (2022) 100087, https://doi.org/10.1016/j.onano.2022.100087.
[61] F. Donsì, M. Annunziata, M. Vincensi, G. Ferrari, Design of nanoemulsion-based delivery systems of natural antimicrobials: Effect of the emulsifier, J. Biotechnol. 159 (2012) 342–350, https://doi.org/10.1016/j.jbiotec.2011.07.001.
[62] C. Shen, H. Liang, Z. Guo, M. Zhang, Members of the histone-derived antimicrobial peptide family from the pearl oyster Pinctada fucata martensii: Inhibition of bacterial growth, Fish Shellfish Immunol. 132 (2023) 108439, https://doi.org/10.1016/j.fsi.2022.11.027.
[63] M.I. Goncheva, D. Chin, D.E. Heinrichs, Nucleotide biosynthesis: the base of bacterial pathogenesis, Trends Microbiol. 30 (2022) 793–804, https://doi.org/10.1016/j.tim.2021.12.007.
[64] R. Njenga, J. Boele, Y. Öztürk, H.-G. Koch, Coping with stress: How bacteria fine-tune protein synthesis and protein transport, J. Biol. Chem. 299 (2023) 105163, https://doi.org/10.1016/j.jbc.2023.105163.
[65] H. Guérin, S. Kulakauskas, M.-P. Chapot-Chartier, Structural variations and roles of rhamnose-rich cell wall polysaccharides in Gram-positive bacteria, J. Biol. Chem. 298 (2022) 102488, https://doi.org/10.1016/j.jbc.2022.102488.
[66] S. Khare, R.K. Singh, O. Prakash, Green synthesis, characterization and biocompatibility evaluation of silver nanoparticles using radish seeds, Results Chem. 4 (2022) 100447, https://doi.org/10.1016/j.rechem.2022.100447.
[67] N. Li, C. Wang, B. Feng, Y. Bi, F. Kong, Z. Wang, S. Tan, Application of nanoencapsulation technology to improve the stability and bioactivity of tea polyphenols, Food Biosci. 55 (2023) 103076, https://doi.org/10.1016/j.fbio.2023.103076.